Journal of Magnetic Resonance **152,** 41–47 (2001)
doi:10.1006/jmre.2001.2400, available online at http://www.idealibrary.com on IDEAL®

Analytical Computation of the Eigenvalues and Eigenvectors in DT-MRI

Khader M. Hasan,*,† Peter J. Basser,‡ Dennis L. Parker,§ and Andrew L. Alexander*,†,¶

*Departments of Medical Physics, ¶Department of Psychiatry, and †W. M. Keck Laboratory for Functional Brain Imaging and Behavior, University of Wisconsin, Madison, Wisconsin 53705-2280; ‡Laboratory of Integrative & Medical Biophysics, National Institutes of Health, Bethesda, Maryland; and §Department of Radiology, University of Utah, Salt Lake City, Utah

E-mail: kmhasan@facstaff.wisc.edu

Received December 4, 2000; revised June 13, 2001

In this paper a noniterative algorithm to be used for the analytical determination of the sorted eigenvalues and corresponding orthonormalized eigenvectors obtained by diffusion tensor magnetic resonance imaging (DT-MRI) is described. The algorithm uses the three invariants of the raw water spin self-diffusion tensor represented by a 3 × 3 positive definite matrix and certain math functions that do not require iteration. The implementation requires a positive definite mask to preserve the physical meaning of the eigenvalues. This algorithm can increase the speed of eigenvalue/eigenvector calculations by a factor of 5–40 over standard iterative Jacobi or singular-value decomposition techniques. This approach may accelerate the computation of eigenvalues, eigenvalue-dependent metrics, and eigenvectors especially when having high-resolution measurements with large numbers of slices and large fields of view.

Key Words: **analytical; diffusion tensor; eigenvalues; eigenvectors.**

INTRODUCTION

A diffusion tensor measurement may be obtained by applying diffusion sensitizing gradient pulses along a minimum of six noncolinear gradient directions for a set diffusion time, gradient strength, and pulse separation (*1–3*). The relationship between the measured diffusion tensor **D** in the scanner frame and the local tissue frame is given by the matrix equation

$$\mathbf{DE} = \mathbf{E\Lambda}. \qquad [1]$$

In Eq. [1] the self-diffusion tensor eigenvalues are the diagonal elements of the matrix $\mathbf{\Lambda}$ and **E** is an orthogonal rotation matrix whose columns are the eigenvectors, $\hat{\mathbf{e}}_\mathbf{i}$, of **D**. There are many useful quantities that can be obtained from the self-diffusion tensor including the trace, measures of diffusion anisotropy, and orientation (*4–6*). For many of these calculations, the eigenvalues and eigenvectors must be computed first. For example, in fiber-tracking applications the accurate determination of the principal eigenvector directions for a large volume is required (*7–10*).

The diffusion tensor matrix can be diagonalized using traditional methods of eigenvector–eigenvalue decomposition (*11*). These methods are usually iterative and, hence, time consuming, especially when performed using interpreted processing languages such as MATLAB or IDL on a voxel-by-voxel basis. The iterative schemes commonly used for symmetric matrix diagonalization include variations of the Jacobi method (*11*) or singular-value decomposition (SVD)-based methods (*11, 12*).

In this paper, we examine an analytical method for calculating eigenvalues, eigenvalue-dependent measures, and eigenvectors of the diffusion tensor directly from the diffusion tensor elements. The efficiency and accuracy of this approach relative to commonly used iterative methods are also investigated.

BACKGROUND AND THEORY

Diffusion Tensor Invariants

The Cartesian diffusion tensor **D** has three principal invariants, $\{I_1, I_2, I_3\}$, which are related to the eigenvalues, $\{\lambda\}$, and defined by the characteristic equation

$$\begin{aligned}\det(\mathbf{D} - \mathbf{\Lambda U_{3\times 3}}) &= (\lambda - \lambda_1)(\lambda - \lambda_2)(\lambda - \lambda_3) \\ &= \lambda^3 - \lambda^2 I_1 + \lambda I_2 - I_3 = 0, \qquad [2]\end{aligned}$$

where $\mathbf{U_{3\times 3}}$ is the 3×3 identity matrix. From this equation, the three invariants are given by (*4, 14*)

$$I_1 = \mathrm{Trace}(\mathbf{D}) = D_{xx} + D_{yy} + D_{zz} = \lambda_1 + \lambda_2 + \lambda_3 \qquad [3]$$

$$\begin{aligned}I_2 &= (D_{xx}D_{yy} + D_{xx}D_{zz} + D_{yy}D_{zz}) - \left(D_{xy}^2 + D_{xz}^2 + D_{yz}^2\right) \\ &= \lambda_1\lambda_2 + \lambda_1\lambda_3 + \lambda_2\lambda_3 \qquad [4]\end{aligned}$$

and

$$\begin{aligned}I_3 = \det(\mathbf{D}) &= D_{xx}D_{yy}D_{zz} + 2D_{xy}D_{xz}D_{yz} \\ &\quad - \left(D_{zz}D_{xy}^2 + D_{yy}D_{xz}^2 + D_{xx}D_{yz}^2\right) = \lambda_1\lambda_2\lambda_3. \qquad [5]\end{aligned}$$

Rotationally Invariant Measures of Diffusion Anisotropy

The three principal tensor invariants can be used to express several anisotropy measures such as relative anisotropy (*4, 5*)

1090-7807/01 $35.00

and fractional anisotropy (*2*). However, for other measures of tensor anisotropy there is no obvious expression for direct analytical calculation from either the diffusion tensor or its invariants. For example, planar and spherical shape measures (*6*) and the cylindrical anisotropy index (*8*) are expressed in terms of the sorted eigenvalues. The analytical solutions for these measures, in terms of either the tensor elements or the three principal tensor rotational invariants, have not been reported. Consequently, the diffusion tensor must be fully diagonalized prior to calculating these measures. As pointed out in the Introduction, the diagonalization can take significant amounts of time and mask the dependency between the measures and the original diffusion tensor.

The Analytical Diagonalization Algorithm

The analytical diagonalization solution presented here is specific to the positive-definite and symmetric Cartesian tensors that are commonly encountered in many applications including diffusion, crystallography, chemical shielding, and continuum mechanics. Descriptions of analytical eigenvalue calculations have been previously documented (*11, 13, 15*). By using the three principal invariants $\{I_1, I_2, I_3\}$ of $\mathbf{D}$ defined above, the following steps lead to the diagonalization of $\mathbf{D}$. In addition, we will obtain an orthonormal eigenvector set, $\mathbf{E}$, that solves Eq. [1].

Determination of the eigenvalues. The following rotationally invariant variables are defined in terms of $\{I_1, I_2, I_3\}$:

$$v = (I_1/3)^2 - I_2/3 \quad [6]$$

and

$$s = (I_1/3)^3 - I_1 I_2/6 + I_3/2. \quad [7]$$

Since for real eigenvalues, $v > 0$ and $s^2 < v^3$, we define

$$\phi = \frac{\operatorname{acos}\left(\frac{s}{v}\sqrt{\frac{1}{v}}\right)}{3}. \quad [8]$$

It should be noted that both v and s variables are related to the second and third rotational invariants of the diffusion deviatoric tensor, $\mathbf{D}_{\text{an}}$, with zero trace or first invariant (*4*):

$$\mathbf{D}_{\text{an}} = \mathbf{D} - I_1/3\mathbf{U}_{\mathbf{3\times 3}}. \quad [9]$$

Thus, we can interpret v and s as variance and skewness measures of $\mathbf{D}_{an}$ respectively,

$$v = \tfrac{1}{6}\,\text{Trace}\left(\mathbf{D}_{\text{an}}^2\right) = \text{Variance}(\lambda) = I_2(\mathbf{D}_{\text{an}})/3 \quad [10]$$

and

$$s = \tfrac{1}{6}\,\text{Trace}\left(\mathbf{D}_{\text{an}}^3\right) = \text{Skewness}(\lambda) = I_3(\mathbf{D}_{\text{an}})/2 = \det(\mathbf{D}_{\text{an}})/2. \quad [11]$$

The sorted eigenvalues ($\lambda_1 > \lambda_2 > \lambda_3$) may now be expressed as

$$\lambda_1 = I_1/3 + 2\sqrt{v}\cos(\phi) \quad [12]$$

$$\lambda_2 = I_1/3 - 2\sqrt{v}\cos(\pi/3 + \phi) \quad [13]$$

and

$$\lambda_3 = I_1/3 - 2\sqrt{v}\cos(\pi/3 - \phi). \quad [14]$$

Note that the eigenvalues need no further sorting due to the cosine function and the fact that $0 \le \phi \le \pi/3$ is assured for a positive-definite DT matrix. The third eigenvalue can also be obtained using the trace invariance property, $\lambda_3 = I_1 - \lambda_1 - \lambda_2$. A discussion of the geometric interpretation of this analytical diagonalization and application to tensor anisotropy is given in the Appendix.

Determination of the eigenvectors. After the sorted eigenvalues have been computed, the ith eigenvector, $\hat{\mathbf{e}}_i = [e_{ix}\ \ e_{iy}\ \ e_{iz}]^{\text{T}}$, may be calculated by solving the linear system of equations, $D\hat{\mathbf{e}}_i = \lambda_i\hat{\mathbf{e}}_i$, for the ratio $e_{ix} : e_{iy} : e_{iz}$. Moreover, the normalization condition, $\hat{\mathbf{e}}_i^{\text{T}}\hat{\mathbf{e}}_i = 1$, can be enforced to determine $\hat{\mathbf{e}}_i$ (*16*). Note that since $-\hat{\mathbf{e}}_i$ is also a solution to the eigenvector problem $D(-\hat{\mathbf{e}}_i) = \lambda_\ell(-\hat{\mathbf{e}}_i)$, a sign ambiguity in the vector direction is unavoidable.

The calculation of the orthonormalized eigenvectors proceeds as follows: for the ith eigenvalue, define the variables

$$A_i = D_{xx} - \lambda_i; \quad B_i = D_{yy} - \lambda_i; \quad C_i = D_{zz} - \lambda_i \quad [15]$$

$$e_{ix} = (D_{xy}D_{yz} - B_i D_{xz})(D_{xz}D_{yz} - C_i D_x) \quad [16]$$

$$e_{iy} = (D_{xz}D_{yz} - C_i D_{xy})(D_{xz}D_{xy} - A_i D_{yz}) \quad [17]$$

and

$$e_{iz} = (D_{xy}D_{yz} - B_i D_{xz})(D_{xz}D_{xy} - A_i D_{yz}). \quad [18]$$

The normalized eigenvector corresponding to λ_i is

$$\hat{\mathbf{e}}_i = \frac{\mathbf{e}_i}{\sqrt{\mathbf{e}_i^{\text{T}}\mathbf{e}_i}}. \quad [19]$$

This procedure may be repeated as desired for $i = 1, 2$, or 3 to obtain the orthonormalized set of eigenvectors that correspond to the major, medium, and minor eigenvalues. Note that the third eigenvector may be obtained more efficiently by the cross product between the other two orthonormal eigenvectors, $\hat{\mathbf{e}}_1$ and $\hat{\mathbf{e}}_2$

$$\hat{\mathbf{e}}_3 = \left[e_{1y}e_{2z} - e_{2y}e_{1z} \quad e_{1z}e_{2x} - e_{1x}e_{2z} \quad e_{1x}e_{2y} - e_{1y}e_{2x}\right]^{\text{T}}. \quad [20]$$

Implementation and algorithm sensitivity issues. The algebraic algorithm presented above can easily be implemented on an entire image volume array. The use of standard math library functions (cos, acos, sqrt, etc.) is the only requirement. There is no need to sort the computed eigenvalues as is generally done when using traditional iterative methods. It is highly advisable to enforce a nonnegative-definite real eigenvalue mask before obtaining the eigenvectors. Prior to eigenvalue determination, the positive-definite mask can be selected to include all voxels that satisfy the necessary and sufficient conditions that assure the convexity of the diffusion ellipsoid (17):

$$I_3 > 0, \quad \text{and} \quad \left(D_{ii} \text{ and } D_{ii}D_{jj} - D_{ij}^2\right) \geq 0 \quad \text{for } i, j = x, y, \text{or } z. \qquad [21]$$

Diffusion measurements usually have some random noise that makes the tissue water diffusivities unique and rarely equal, even for a water phantom, as will be demonstrated experimentally. Additionally, the enforcement of this positive-definite mask assures that

$$(\lambda_1, \lambda_2, \text{ and } \lambda_3) > 0, \qquad [22]$$

which will reduce the chance of division by 0 in Eq. [19] above. The mask will remove air and very-low-signal regions. Note also that this mask will not remove a voxel with degenerate eigenvalues. This case corresponds to $\nu = 0$ in Eq. [10] and is extremely rare even at the highest available SNR on an isotropic water phantom.

MATERIALS AND METHODS

DT-MRI Experiments

Diffusion tensor image measurements were obtained from a normal human subject using a single-shot spin-echo prepared EPI pulse sequence on a 1.5-T SIGNA MRI scanner (General Electric) with NV/CVi gradients (maximum gradient amplitude = 4 G/cm). Informed consent was obtained as per the guidelines of the Institutional Review Board. Single axial slices with image matrix = 128 × 128 were acquired with FOV = 24 cm. The total number of images, $N_t = 55$, was partitioned into reference images of $N_{ref} = 7$ ($b = 0$), and $N_e = 6$ encoding directions, each averaged $N_d = 8$ times ($N_t = N_{ref} + N_e N_d$). The echo time, TE; repetition time, TR; diffusion pulse duration, δ; and separation, Δ, are TE/TR/δ/Δ = 94/2000/23/29 ms, with slice thickness = 4 mm. The diffusion weighting b-factor is $b = 1341$ s mm^{-2}. The diffusion tensor encoding scheme used six noncolinear directions of the scaled icosahedron (Icosa6) (*18, 19*) on a unit sphere (i.e., $\{G_x, G_y, G_z\} = G_{max}/\sqrt{\tau^2 + 1} \times \{[\tau\ 1\ 0], [\tau\ -1\ 0], [0\ 1\ \tau], [0\ \tau\ -1], [1\ \tau\ 0], \text{and } [-1\ 0\ \tau]\}$, where $\tau = (\sqrt{5} - 1)/2$ and $G_{max} = 4$ G/cm.

Water phantom measurements were also acquired using the icosahedral encoding scheme, at a higher signal-to-noise ratio, to examine the sensitivity of the eigenvector and eigenvalue solutions as provided by the analytical approach. The total number of images, $N_t = 134$, was partitioned into reference images of $N_{ref} = 8$, with encoding directions, $N_e = 6$, each averaged $N_d = 21$ times. The echo time, TE; repetition time, TR; diffusion pulse duration, δ; and separation, Δ, are TE/TR/δ/Δ = 72/5500/16/23 ms, with slice thickness = 5 mm. The gradient strength, G, was tuned to achieve a diffusion b-factor of approximately 500 s mm^{-2}.

For both the brain and water imaging studies, the eigenvalues and eigenvectors were calculated using three diagonalization methods: (1) the conventional iterative Jacobi-QL (J-QL) method (*16*), (2) singular-value decomposition, and (3) the analytical method described in Eqs. [12]–[14] and [15]–[18]. All diagonalization methods used the same positive-definite mask defined by Eqs. [21].

RESULTS

Computational Efficiency

The analytical algorithm was implemented on a UNIX workstation (Sun4-Sol2@360 MHz Sparcv9 processor) in the C programming language. The results given by the analytical algorithm Eqs. [12]–[20] were compared with those obtained using the eigen decomposition routine (qr.c, jacobi.c, and svdcmp.c) in "Numerical Recipes in C" (*11*). The (qr.c) routine was optimized for symmetric matrices. The analytical code gave a rough computational advantage factor of 5 over the qr.c algorithm (8 vs 44 s) for a total number of $N = 1{,}000{,}000$ of randomly generated positive definite 3 × 3 matrices.

The analytical algorithm was also implemented using MATLAB-r11 (Mathworks, Inc., Natick, MA, version 5.3) and IDL (Research Systems, Inc., Boulder, CO, version 5.3) languages on the same workstation for a 128 × 128 × 6 diffusion array. For MATLAB with double-precision computation, the proposed analytical approach provided the positive-definite mask array, three eigenvalue and eigenvector arrays in less than 0.4 s versus 15.8 s using the iterative voxel-by-voxel built-in routine, eig.m, and 12 s for the svd.m routine. For IDL, the results were 0.5 s using the analytical algorithm versus 2.8 s using the eigenql.pro code. Hence, the computation time advantage factor on the whole image array is approximately 30–40 using MATLAB, and 6 using IDL with the quoted routines.

Brain Water Self-Diffusion Imaging

Maps of the relative eigenvalue differences

$$|\lambda_i - \lambda_a|/\lambda_i \qquad [23]$$

between the analytical and the iterative (J-QL method) calculations were computed (not shown). These maps showed that the eigenvalue calculation does not appear to depend significantly on the method of computation. One interesting observation

is that the relative difference is lowest for regions of highly anisotropic white matter. However, for more isotropic regions the largest relative difference is on the order of 5×10^{-15}, which is negligible for practical considerations. This difference may be attributed to the lower stability of the eigenvalue decomposition for less anisotropic regions, such as in gray matter (GM) and the cerebrospinal fluid (CSF). In white matter (WM), the noise/sorting bias for λ_1 is less severe than in isotropic regions.

The analytical and iterative calculations of the eigenvectors were also compared. A map of the absolute dot products, $|\hat{\mathbf{e}}_a^{\mathrm{T}}\hat{\mathbf{e}}_i|$, was identical to the binary positive definite mask, which indicates that the analytical approach provides the same set of directions as the iterative approach.

Another way to evaluate the accuracy of the diagonalization is to compute the difference between the original measured tensor data and the tensor constructed from the computed eigenvectors and eigenvalues. This approach may be used to determine which method is most accurate for these calculations. A measure of the error norm (ERR) is defined as

$$\mathrm{ERR} = \frac{\sqrt{I_4(\mathbf{E}\boldsymbol{\Lambda}\mathbf{E}^{\mathrm{T}} - \mathbf{D}_{\mathrm{True}})}}{\sqrt{I_4(\mathbf{D}_{\mathrm{True}})}}, \qquad [24]$$

where $\mathbf{D}_{\mathrm{True}}$ is the measured diffusion tensor, $\mathbf{E}$ and $\boldsymbol{\Lambda}$ are the estimated eigenvector and eigenvalue matrices, I_4 is a fourth invariant (14),

$$\begin{aligned} I_4 &= \mathrm{Trace}(\mathbf{D}^2) = D_{xx}^2 + D_{yy}^2 + D_{zz}^2 + 2\left(D_{xy}^2 + D_{xz}^2 + D_{yz}^2\right) \\ &= I_1^2 - 2I_2. \end{aligned} \qquad [25]$$

Figure 1 maps this error quantity for the SVD, J-QL, and analytical calculation methods. The error for the analytical approach appears lowest for regions with high anisotropy (white matter). The ranges for these maps were scaled for display. The actual maximum error was roughly 2.0×10^{-15}, 3.0×10^{-15}, and 2.5×10^{-9}, for the iterative SVD, the J-QL, and the analytical methods respectively. Note that the analytical error occurred for a single voxel at this level. This voxel corresponded to a nearly isotropic voxel in the CSF and corresponded to the largest ERR value for all methods. All other image voxels had errors at least two orders of magnitude lower. In general, the SVD method appears most accurate, followed by the J-QL method, and the analytical method was the least accurate. It should be noted that both iterative techniques (SVD and J-QL) use a convergence criterion similar to Eq. (24). Despite a difference in the calculated errors on the order of four to six orders of magnitude, the overall relative error for all methods is negligible for most applications.

Aqueous Phantom Diffusion Tensor Imaging

The brain imaging results demonstrated that error associated with tensor feature estimates is greatest in primarily isotropic regions. Therefore, an aqueous solution phantom, which has isotropic diffusion properties, should also demonstrate significant error differences between the techniques. The error measure in Eq. [24] was applied to calculations of eigenvalues and eigenvectors for the water phantom imaging studies. The results are shown in Fig. 2. The displayed gray levels have been scaled. The true maximum values are roughly 1.5×10^{-16}, 2.5×10^{-16}, and 10^{-8}, for the SVD, J-QL, and analytical techniques respectively. Again, the SVD appears most accurate, although the relative error for all the calculation methods is practically negligible. The analytical technique depicts a centered dark horizontal stripe on the error map, which was puzzling at first. Closer investigation of the image data showed a low amplitude zipper artifact in this region that may have yielded a small, yet artificial increase in the anisotropy.

Relative eigenvalue difference (Eq. [23]) and eigenvector dot-product maps were also generated (not shown), which compared the eigenvalue and eigenvector results for the J-QL and the Analytical methods. The maximum relative eigenvalue difference was on the order of 10^{-12}. The absolute eigenvector dot product was also unity everywhere within the phantom. Note that for the ideal degenerate (isotropic) diffusion tensor, any orthonormal vector is a valid solution. The stability of the algorithm is explained in part by the fact that the likelihood of encountering a degenerate case is very small in the presence of noise.

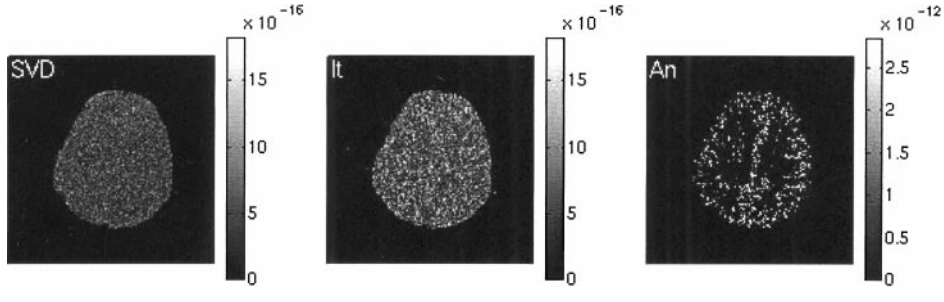

FIG. 1. Tensor relative error (ERR) maps for the SVD, the J-QL (It), and the analytical tensor (An) diagonalization methods for the human brain tensor measurements.

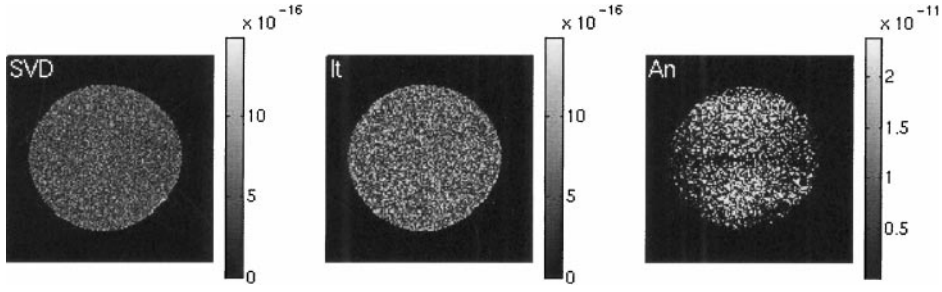

FIG. 2. Tensor relative error (ERR) maps for the SVD, the J-QL (It), and the analytical tensor (An) diagonalization methods for the aqueous phantom.

DISCUSSION

The results of this study demonstrate that an analytical diagnonalization approach is stable and accurate enough for most DT-MRI applications. Although the error for the analytical approach is greater than either of the iterative techniques, the amount of error detected in the images is much smaller than the effects of measurement noise. In all imaging studies, including others not described in this study, the eigenvalue and eigenvector images generated using all of the diagnonalization techniques were visually identical. The analytical technique will fail when the tensor has either degenerate or nonpositive eigenvalues. Consequently, it is critical to detect and mask these voxels as described under Background and Theory. In general, iterative methods were developed for tensor diagonalization because they were more accurate and stable than direct algebraic calculations. However, the main cost of these iterative approaches is compromised computational speed.

As described previously, certain measures of tensor anisotropy such as the linear and planar tensor shape measures and the cylindrical anisotropy index are normally written in terms of the eigenvalues. By using direct algebraic diagonalization, these anisotropic measures can now be expressed algebraically in terms of the tensor elements (*20*). The relationships for these measures are described in the Appendix.

The improved speed of this direct algebraic diagonalization will be useful for analyzing large DT-MRI data sets, such as those obtained for white matter tractography applications. Another application of this method is for error analysis in DT-MRI. Currently, iterative statistical procedures such as Monte Carlo and bootstrap techniques *(2, 21–24)* are used to estimate the effects of measurement noise on DT-MRI derived parameters, such as the trace values, anisotropy values, and eigenvector directions. These statistical procedures may be greatly accelerated by using analytical diagonalization. Alternatively, since these measures can now be expressed directly in terms of the tensor invariants and tensor elements, the effects of measurement noise on the measures can also be determined analytically. Consequently, noise effects can now be predicted without time-consuming iterative techniques.

APPENDIX

Geometric Interpretation of the Analytical Diagonalization

The analytical diagonalization of the a second-order positive definite tensor may be described geometrically using a trilinear coordinate system (*12, 13, 15, 25*). The trilinear coordinates for describing the tensor eigenvalues is illustrated in Fig. A1. This system consists of an equilateral triangle of unit latitude with the trace-weighted eigenvalues at the vertices. In this coordinate system any diffusion tensor can be described by the aspherism index, A (the distance from the centroid of the triangle (*26*)) and the angle ϕ, which is defined in Eq. [8]. Note that this system is different from either the barycentric tensor shape diagram that we used previously to define tensor shape (*27*) or the coordinate systems described by Bahn (*28*). The perpendicular distance opposite of each side is defined in terms of the sorted positive eigenvalues as

$$x_i = \lambda_i / I_1. \qquad [A1]$$

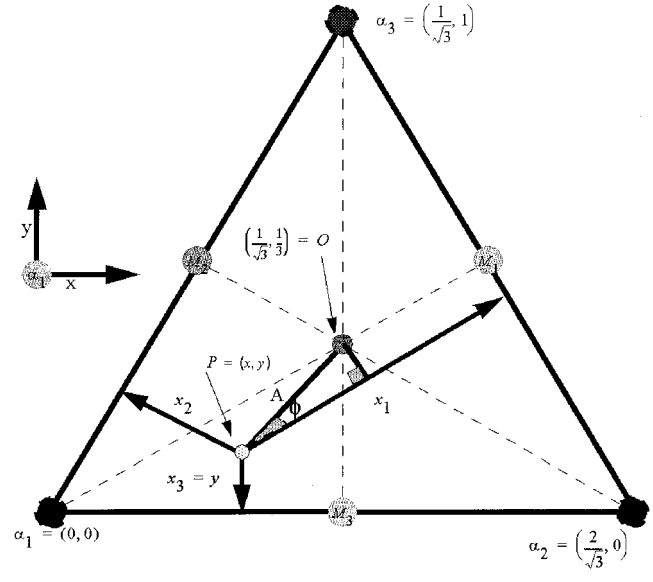

FIG. A1. Illustration of the trilinear coordinate system that is used to describe diagonalization of the tensor eigenvalues.

Properties of the coordinate system include

$$x_3 = y \quad \text{and} \quad x_1 + x_2 + x_3 = 1 \qquad [A2]$$

$$O\alpha_i = 2/3; \quad OM_i = 1/3 \quad \text{for } i = 1, 2, 3, \qquad [A3]$$

where O is the triangle centroid, α_i are the triangle vertices, M_i are the edge bisectors. The two-dimensional Cartesian coordinates (x, y) of any point P in the triangle can be expressed using straightforward geometry by the transformation,

$$[x \quad y] = [(1 - x_1 + x_2)/\sqrt{3} \quad 1 - x_1 - x_2]. \qquad [A4]$$

The distance OP is known as the aspherism index, A, which is related to the relative anisotropy by

$$A = OP = \sqrt{[(x - 1/\sqrt{3})^2 + (y - 1/3)^2]} = 2/3\,\mathrm{RA}, \qquad [A5]$$

where RA is given in terms of the first two principal invariants as

$$\mathrm{RA} = \sqrt{1 - \frac{3I_2}{{I_1}^2}}. \qquad [A6]$$

The graph can also be used to provide a geometric derivation of the eigenvalues and anisotropy indices. By using the angle ϕ (Fig. A1), we note that

$$x_i = OM_i + A\cos(\phi). \qquad [A7]$$

Similarly, in terms of I_1, RA, and ϕ, we can express the eigenvalues in terms of the vector equation

$$\begin{bmatrix} \lambda_1 \\ \lambda_2 \\ \lambda_3 \end{bmatrix} = \frac{I_1}{3}\left(1 + 2\,\mathrm{RA}\begin{bmatrix} \cos\phi \\ -\cos\left(\frac{\pi}{3} + \phi\right) \\ -\cos\left(\frac{\pi}{3} - \phi\right) \end{bmatrix}\right). \qquad [A8]$$

Algebraic Expressions of Anisotropy Measures

Several anisotropy measures of the diffusion tensor, such as the cylindrical anisotropy index

$$A_{\mathrm{cyl}} = [\lambda_1 - (\lambda_2 + \lambda_3)/2]/I_1 \qquad [A9]$$

and the linear and planar shape measures

$$\mathrm{CL} = (\lambda_1 - \lambda_2)/I_1 \qquad [A10]$$

$$\mathrm{CP} = 2(\lambda_2 - \lambda_3)/I_1, \qquad [A11]$$

are generally expressed in terms of the eigenvalues, which required diagonalization. The set of equations in [A8] can now be used to algebraically express these anisotropy measures in terms of RA and ϕ as follows:

$$A_{\mathrm{cyl}} = \mathrm{RA}\cos(\phi) \qquad [A12]$$

$$\mathrm{CL} = 2\,\mathrm{RA}\frac{\sin\left(\frac{\pi}{3} - \phi\right)}{\sin\left(\frac{\pi}{3}\right)} \qquad [A13]$$

$$\mathrm{CP} = 2\,\mathrm{RA}\frac{\sin(\phi)}{\sin\left(\frac{\pi}{3}\right)}. \qquad [A14]$$

Consequently, these measures can be computed without diagonalization.

ACKNOWLEDGMENTS

We thank Dr. R. I. Shrager for his critical reading of the manuscript and the constructive comments made on the eigenvector sensitivity to degenerative cases and on round-off errors, and for suggesting the tensor norm. K. M. Hasan thanks J. A. Roberts for programming assistance, and Drs. G. Gullberg, G. A. Williams, and C. Goodrich for encouragement. The authors also thank Sean Webb and Marci A. Harris for editorial assistance. This work is funded by NIH Grants R01 MH62015 and P30 CA42014.

REFERENCES

1. P. J. Basser, J. Mattiello, and D. Le Bihan, Estimation of the effective self-diffusion tensor from the NMR spin echo, *J. Magn. Reson. B* **103,** 247–254 (1994).
2. C. Pierpaoli and P. J. Basser, Toward a quantitative assessment of diffusion anisotropy, *Magn. Reson. Med.* **36,** 893–906 (1996).
3. P. J. Basser and C. Pierpaoli, A simplified method to measure the diffusion tensor from seven MR images, *Magn. Reson. Med.* **39,** 928–934 (1998).
4. P. J. Basser, New histological and physiological stains derived from diffusion-tensor MR images, *Ann. N.Y. Acad. Sci*. **820,** 123–138 (1997).
5. T. E. Conturo, R. C. McKinstry, E. Akbudak, and B. H. Robinson, Encoding of anisotropic diffusion with tetrahedral gradients: A general mathematical diffusion formalism and experimental results, *Magn. Reson. Med*. **35,** 399–412 (1996).
6. C. F. Westin, S. Peled, H. Gudbjarsson, R. Kikinis, and F. A. Jolesz, Geometrical diffusion measures for MRI from tensor basis analysis, Abstracts of the International Society of Magnetic Resonance in Medicine, 5th Annual Meeting, p. 1742, Vancouver (1997).
7. P. J. Basser, S. Pajevic, C. Pierpaoli, J. Duda, and A. Aldroubi, In vivo fiber-tractography using diffusion DT-MRI, *Magn. Reson. Med*. **44,** 625–632 (2000).
8. C. Poupon, C. A. Clark, V. Frouin, J. Regis, I. Bloch, D. Le Bihan, and J. Mangin, Regularization of diffusion-based direction maps for the tracking of brain white matter fascicles, *Neuroimage* **12,** 184–195 (2000).
9. T. E. Conturo, N. F. Lori, T. S. Cull, *et al.*, Tracking neuronal fiber pathways in the living human brain, *Proc. Natl. Acad. Sci*. **96,** 10,422–10,427 (1999).
10. S. Mori, W. E. Kaufmann, G. D. Pearlson, B. J. Crain, B. Stieltjes, M. Solaiyappan, and P. C. van Zijl, In vivo visualization of human neural pathways by magnetic resonance imaging, *Ann Neurol.* **47,** 412–414 (2000).
11. W. H. Press, B. P. Flannery, F. A. Teukolsky, and W. T. Vetterling, "Numerical Recipes in C," Cambridge Univ. Press, Cambridge (1997).
12. E. R. Malinowski, "Factor Analysis in Chemistry," p. 350, Wiley, New York (1991).

13. E. W. Weisstein, "CRC Concise Encyclopedia of Mathematics," pp. 362–365, 884, and 1859–1860, CRC Press, Boca Raton, FL (1999).

14. A. I. Borisenko and I. E. Tarapov, "Vector and Tensor Analysis with Applications," pp. 121–122, Dover, New York (1968).

15. D. M. Burton, "History of Mathematics: An Introduction," 3rd ed., pp. 286–300, McGraw-Hill, New York (1997).

16. K. R. Symon, "Mechanics," 2nd ed., pp. 403–425, Addison-Wesley, Reading, MA (1960).

17. R. E. Bellman, "Introduction to Matrix Analysis," p. 74, McGraw-Hill, New York (1960).

18. R. Muthupallai, C. A. Holder, A. W. Song, and W. T. Dixon, Navigator-aided, multishot EPI diffusion images of brain with complete orientation and anisotropic information, Abstracts of the International Society of Magnetic Resonance in Medicine, 7th Annual Meeting, p. 1825, Philadelphia (1999).

19. K. M. Hasan, D. L. Parker, and A. L. Alexander. Comparison of gradient encoding schemes for diffusion-tensor imaging. *J. Magn. Reson. Imaging* **13,** 769–780 (2001).

20. A. M. Ulug and P. C. van Zijl, Orientation-independent diffusion imaging without tensor diagonalization: Anisotropy definitions based on physical attributes of the diffusion ellipsoid, *J. Magn. Reson. Imaging* **9,** 804–813 (1999).

21. P. J. Basser, Quantifying errors in fiber-tract direction and diffusion tensor field maps resulting from MR noise, Abstracts of the International Society of Magnetic Resonance in Medicine, 5th Annual Meeting, p. 1740, Vancouver (1997).

22. M. E. Bastin, P. A. Armitage, and I. Marshall, A theoretical study of the effect of experimental noise on the measurement of anisotropy in diffusion imaging, *Magn. Reson. Imaging* **16,** 773–778 (1998).

23. S. Pajevic and P. J. Basser, Non-parametric statistical analysis of diffusion tensor MRI data using the bootstrap method, Abstracts of the International Society of Magnetic Resonance in Medicine, 7th Annual Meeting, p. 1790, Philadelphia (1999).

24. K. M. Hasan, D. L. Parker, and A. L. Alexander. Bootstrap analysis of DT-MRI encoding techniques, Abstracts of the International Society of Magnetic Resonance in Medicine, 8th Annual Meeting, p. 789, Denver (2000).

25. D. E. Sands, "Vectors and Tensors in Crystallography," pp. 138–139, Dover, New York (1982).

26. D. Weigel, T. Beguesmi, P. Garnier, and J. F. Berar, Evolution des tensuers de dilatation thermique en fonction de la temperature, *J. Solid State Chem.* **23,** 241–251 (1978).

27. A. L. Alexander, K. M. Hasan, G. Kindlmann, D. L. Parker, and J. S. Tsuruda, A geometric analysis of diffusion tensor measurements of the human brain, *Magn. Reson. Med.* **44,** 283–291 (2000).

28. M. M. Bahn, Invariant and orthonormal scalar measures derived from magnetic resonance diffusion tensor imaging, *J. Magn. Reson.* **141,** 68–77 (1999), doi: 10.1006/jmre.1999.1875.